Journal of Catalysis 259 (2008) 190–202

Contents lists available at ScienceDirect

Journal of Catalysis

www.elsevier.com/locate/jcat

Methylcyclohexane transformation over HMCM22 zeolite: Mechanism and location of the reactions

P. Matias [a,b], J.M. Lopes [a], S. Laforge [b], P. Magnoux [b], P.A. Russo [c], M.M.L. Ribeiro Carrott [c], M. Guisnet [a,b,*], F. Ramôa Ribeiro [a,*]

[a] IBB—Institute for Biotechnology and Bioengineering, Centre for Biological and Chemical Engineering, Instituto Superior Técnico, Av. Rovisco Pais, 1049-001 Lisboa, Portugal
[b] LACCO, UMR CNRS 6503, 40, Avenue du Recteur Pineau, 86022 Poitiers Cedex, France
[c] Centro de Química de Évora and Departamento de Química, Universidade de Évora, Colégio Luís António Verney, Rua Romão Ramalho 59, 7000-671 Évora, Portugal

ARTICLE INFO

Article history:
Received 15 April 2008
Revised 1 August 2008
Accepted 13 August 2008

Keywords:
MCM-22 zeolite
Methylcyclohexane transformation
Isomerisation
Cracking
Coking
Reactions
Location
Mechanisms

ABSTRACT

At 350 °C, over a HMWW zeolite (Si/Al = 14.5), methylcyclohexane (mch) transforms into four types of products: isomers (I), C_1–C_8 aliphatic hydrocarbons (C), benzenic hydrocarbons (A), and trapped carbonaceous compounds (coke). The role played by the various micropores was established through a two-step method: deactivation of supercages by coking and poisoning of the outer hemicage sites by 2,4-dimethylquinoline. More than 85% of mch transformation occurs in the supercages, ~11% occurs in the outer hemicages, and only <2% occurs in the sinusoidal channels, which, considering the protonic site distribution, corresponds to turnover frequency values of 33, 82, and 2 h^{-1}. The product distributions are very different: I, C_3–C_5 branched alkanes, and coke in similar amounts; essentially I and C_3–C_8 branched alkanes; and mainly C_1–C_8 and A products. The carbenium ion chain mechanism can account for the products formed in supercages and hemicages, whereas protolytic mechanisms play an important role in the narrow sinusoidal channels. Deactivation by coking is very fast in supercages and negligible in the other locations.

1. Introduction

The MCM22 zeolite (MWW) has a very original structure composed of two independent 10 MR pore systems [1]: large supercages with 12 MR inner diameter of 7.1 Å and height of 18.2 Å connected by openings of 4.1 × 5.5 Å and bidimensional sinusoidal channels (4.1 × 5.1 Å), with intersections of 6.4 × 6.9 Å. Moreover, the outer surfaces of crystals have large 12 MR pockets that correspond to half supercages (diameter, 7.1 Å; height, 7.0 Å) [2,3].

The presence of these outer hemicages could explain why the catalytic behaviour of HMCM22 samples often is found to be intermediate between those of large- and medium-pore zeolites [4–6]. Indeed, because there are protonic sites in the inner pore systems (supercages and sinusoidal channels) and outer hemicages, acid-catalysed reactions can occur in the three locations.

With certain reactions over chosen HMCM22 samples, one of the pore systems can play a major catalytic role. Thus, toluene disproportionation has been shown to selectively yield the slimmer *para* xylene isomer, demonstrating that this reaction occurs preferentially within the shape-selective 10 MR inner micropores [7–9]. Moreover, because this reaction requires bulky bimolecular intermediates, which cannot be accommodated within the narrow sinusoidal channels (even at their intersection), it has been concluded that toluene disproportionation occurs within the large supercages [7–9]. But a predominant role of the supercages cannot be deduced from the high *para* selectivity of ethylbenzene disproportionation [10,11]; indeed, in intermediate-pore size zeolites without cages (e.g., MFI [12]), and thus in the MCM22 sinusoidal channels, this reaction can proceed through a deethylation–ethylation mechanism, that is, without participation of bulky intermediates. Likewise, selective toluene alkylation with methanol into *para*-xylene [13] and selective cyclopentene hydration (i.e., limited formation of the undesired bimolecular products such as dicyclopentyl ether) can occur only within the inner micropores [14], but again, because these reactions do not require very bulky intermediates, the respective role of supercages and sinusoidal channels cannot be specified.

In contrast, the absence of shape selectivity in the liquid-phase alkylation of phenol with *tert*-butanol over HMCM22 (no enhanced selective production of *para-tert*-butyl phenol) demonstrates that this reaction does not occur in the inner micropores, and thus is

* Corresponding authors at: IBB—Institute for Biotechnology and Bioengineering, Centre for Biological and Chemical Engineering, Instituto Superior Técnico, Av. Rovisco Pais, 1049-001 Lisboa, Portugal. Fax: +351 21 841 9198.
E-mail addresses: michel.guisnet@univ-poitiers.fr (M. Guisnet), ramoa.ribeiro@ist.utl.pt (F. Ramôa Ribeiro).

0021-9517/$ – see front matter
doi:10.1016/j.jcat.2008.08.006

catalysed by the outer sites [15]. Likewise, the selective and stable production of ethylbenzene and of cumene over the HMCM22 zeolite (Mobil/Raytheon EBMax and Mobil-Badger commercial processes, respectively [3,16,17]) can only be explained by catalysis over the protonic sites of the outer hemicages.

A good way to confirm the preferential catalytic role of the inner micropores or the outer hemicages is to selectively poison the external protonic sites by bulky basic molecules or to passivate or dealuminate the outer surface [7,9,11,14,18–23]. At least for reactions carried out at relatively low temperatures, selective poisoning is the best method. Indeed, in contrast to the other methods, it allows the complete deactivation of the outer acidic sites. Therefore, the relative roles of the inner micropores and the outer hemicages in the reaction can be determined quantitatively [22].

An important observation is that deactivation, which occurs essentially by coking, affects the protonic sites of the three types of micropores in different ways. Thus, the alkylation of benzenic hydrocarbons with propene becomes selective in the desired products only after deactivation of the inner micropores. C_4–C_6 olefinic side products resulting from oligomerisation cracking of propene can be observed on the fresh sample [23]. Therefore, the role played by the various micropores must be established for different degrees of deactivation, that is, for different values of time on stream.

The very significant difference in the sensitivity to deactivation by coking of the MCM22 pore systems was used to develop a simple method for discriminating between the catalytic roles played by the supercages and the sinusoidal channels [22]. This method involves deactivating completely and selectively the protonic sites of the supercages by carbonaceous compounds (coke), which is possible by ageing the zeolite during *m*-xylene transformation at 350 °C for 10 h. With this reaction and under these conditions, carbonaceous deposits accumulate rapidly within the supercages, due to a trapping effect [24]. Indeed, in these large supercages, *m*-xylene can undergo successive reactions leading to products too bulky to diffuse through the narrow apertures, which thus deactivate the protonic sites by poisoning or/and blockage. In contrast, there is practically no coke formation, and thus no deactivation of the sinusoidal channels and of the outer hemicages. In the first case, steric constraints inhibit the formation of products sufficiently bulky to be trapped, whereas in the second case, the primary reaction products are easily desorbed; therefore, successive secondary reactions leading to carbonaceous products are not possible [24].

By coupling supercage deactivation by coking and poisoning with 2,4-dimethylquinoline, the catalytic role played by the three pore systems of MCM22 zeolites can be determined quantitatively. This was done previously for the transformation of the three xylene isomers [25] and for toluene alkylation with propene [23], that is, for reactions involving relatively basic molecules capable of chemisorbing and reacting on relatively weak acidic sites.

In this paper, the same procedure is applied to the transformation of methylcyclohexane over a HMCM22 sample at 350 °C. The catalytic role of the three types of micropores was specified and mechanisms were proposed for the formation of the main reaction products. The originality with respect to the transformation of xylenes (reactants with similar molecular sizes) is that methylcyclohexane is a nonbasic reactant; thus, the activity of the acidic sites of the three pore systems may depend more on their strength. Moreover, the acid-catalysed methylcyclohexane transformation system is more complex than xylene transformations: numerous primary and secondary reactions can occur [26] with the possible co-participation of the acid sites of the pore systems.

2. Experimental

2.1. Synthesis and characterisation of the MCM-22 sample

The MCM-22 precursor was synthesised following the procedure described in the literature [27] and using hexamethyleneimine as a structure-directing agent, submitted to calcination under dry air flow at 580 °C for 12 h to form the MCM-22 structure [2], then exchanged twice with a 2 M NH_4NO_3 solution under reflux at 80 °C for 1 h, and calcined under dry air flow at 500 °C for 4 h to obtain the HMCM22 sample.

The precursor and zeolite samples were characterised by X-ray powder diffraction (XRD) on a Bruker D8 Advance diffractometer with a graphite monochromator using a Cu$K\alpha$ radiation ($\lambda = 1.5406$ Å). Scanning electron microscopy (SEM) was used to evaluate the crystallite size and morphology of the HMCM22 zeolite. The chemical composition (Si, Al, and Na) of HMCM22 was obtained by elemental analysis with atomic emission spectrometry (ICP-AES), and the carbon content of coked samples was determined by total combustion (Fisons Instruments EA 1108).

Nitrogen adsorption measurements were carried out at 77 K with a Micromeritics ASAP 2000 apparatus. Before adsorption, the fresh HMCM22 sample was pretreated at 350 °C under vacuum for 6 h, whereas coked samples were submitted to a milder pretreatment (under vacuum at 100 °C for 2 h) to prevent coke removal. The micropore volume (pore diameter <20 Å) (V_{tp}) and the external surface (S_{ext}) were both estimated by the *t*-method [28] using the Harkins–Jura equation [29]. The Dubinin–Radushkevich equation [30] also was applied to estimate the micropore volume (V_{DR}). Adsorption studies with *p*-xylene also were carried out at 298 K. The *p*-xylene vapour adsorption isotherms were determined gravimetrically in an apparatus equipped with a CI Electronics MK2 vacuum microbalance and an Edwards Barocel 622 capacitance manometer (0–100 mbar). The temperature of the circulating liquid jacket around the balance tubes was controlled within ±0.1 K using a Grant LTD thermostat and a Masterflex peristaltic pump. The liquid *p*-xylene (99%, Fluka) was outgassed in the vacuum rig by repeated freeze-thaw cycles before the isotherms were determined. The effective micropore volume for *p*-xylene was estimated by applying the α_s method in the usual manner [31], with the *p*-xylene isotherm determined on nonporous silica TK800 used as a reference.

The conditions used for determining the acidity of the zeolite samples by pyridine and 2,4-dimethylquinoline (2,4-DMQ) chemisorption followed by FTIR spectroscopy were described previously [32,33]. Identification of the coke components was carried out as described previously [34] based on dissolution of the zeolite matrix in a 40% hydrofluoric acid solution, neutralisation of the obtained aqueous solution with $NaHCO_3$, extraction of organic components from this solution with methylene chloride, and then mass spectrometry analysis (GC/MS coupling).

2.2. Catalytic tests

The catalytic tests were carried out at 350 °C and atmospheric pressure in a Pyrex fixed-bed reactor containing the zeolite sample pretreated in situ at 450 °C under nitrogen flow (60 mL/min) for 8 h. The liquid reactant was injected at a constant rate with a B-Braun Secura perfusor. The reaction products were collected with a 10-position valve (supplied by VICI) and analysed online with a Shimadzu GC-14B gas chromatograph equipped with a Chrompack Plot Al_2O_3/KCl capillary column (50 m) and a flame ionisation detector. Effluent samples were collected for different time on stream values, with the first value corresponding to the time needed to achieve stable reactant pressure. After reaction, the catalyst was

Table 1
Physicochemical characteristics of the HMCM-22 zeolite sample

Textural parameters		Acid site distribution (μmol g^{-1})		
V_{DR} (cm^3 g^{-1})	0.22	C_{Bt}[a]	C_{Lt}[a]	C_{Bext}
		654	128	25[b]; 20–25[c]
V_{mp} (cm^3 g^{-1})	0.19	Relative distribution of bridging OH groups (%)[d]		
S_{ext} (m^2 g^{-1})	91	Supercages	Sinusoidal channels	Hexagonal prisms
		71	19	10

V_{DR}, micropore volume estimated using the Dubinin–Radushkevich equation; V_{mp}, micropore volume obtained by the t-method; S_{ext}, external surface obtained by the t-method. Acidity:
[a] Total concentration of Brønsted and Lewis acid sites (C_{Bt}, C_{Lt}) determined by pyridine adsorption at 150 °C followed by IR spectroscopy.
[b] Concentration of external Brønsted sites (C_{Bext}) determined by 2,4-DMQ adsorption at 200 °C followed by IR spectroscopy.
[c] Concentration of external Brønsted sites (C_{Bext}) determined by 2,4-DMQ adsorption at 200 °C followed by poisoning experiments.
[d] Distribution of bridging OH groups determined by deconvolution of the band at 3620 cm^{-1} according to [35].

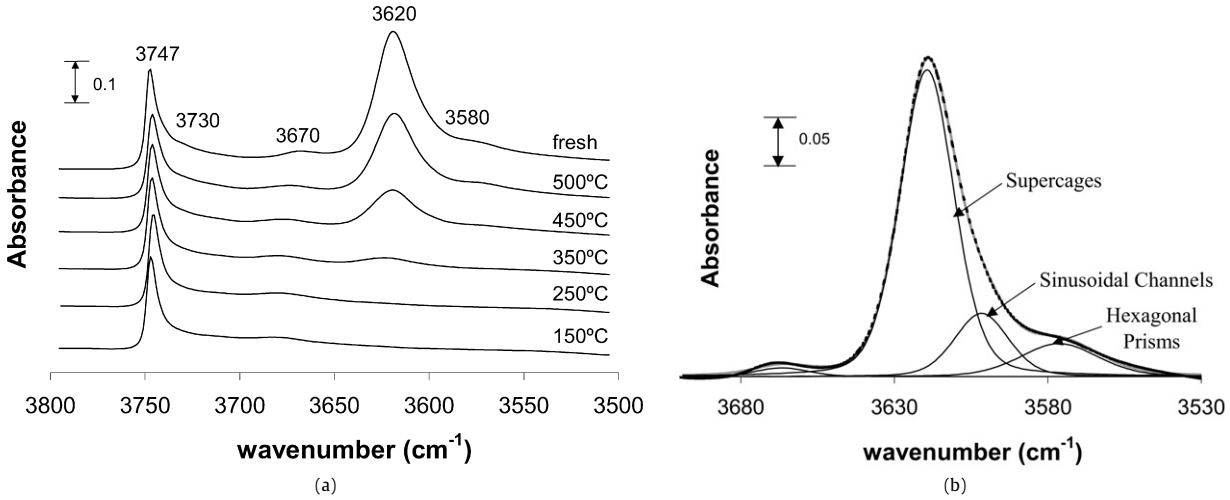

Fig. 1. (a) IR spectra of the HMCM-22 sample in the OH-stretching region before pyridine adsorption (fresh) and after pyridine evacuation at 150 °C, 250 °C, 350 °C, 450 °C and 500 °C, respectively. (b) Deconvolution of the OH band at 3620 cm^{-1} corresponding to bridging hydroxyl groups able to retain pyridine adsorbed at 150 °C.

rapidly cooled to room temperature under nitrogen flow and kept in the refrigerator, to avoid coke modification.

The following conditions were used for methylcyclohexane (mch) transformation (99%, Merck): 350 °C, $p_{mch} = 0.14$ atm, N_2/MCH molar ratio of 6. The contact time (taken as the reverse of the weight hourly space velocity [WHSV]) was varied from 0.0325 to 0.13 h by changing the mass of the catalyst (from 75 mg to 300 mg) and keeping the reactant flow constant (3 mL/h).

The following procedure was used to estimate the role of the three pore systems in mch transformation: (1) reaction with *m*-xylene (percolated on a silica gel column to eliminate traces of peroxide) for 10 h in the following conditions: $p_{m\text{-xylene}}/p_{N_2}$, 13; molar flow of *m*-xylene, 2 mL/h; (2) transformation of pure mch for 1 h; and then (3) of mch added with 2,4-dimethylquinoline (2,4-DMQ) for 2 h, with the concentration of this base ($Q_{2,4\text{-DMQ}} =$ 207 μmol g^{-1} h^{-1}) being sufficiently high to poison all of the outer acid sites in less than 10 min.

3. Results and discussion

3.1. Physicochemical characteristics of the HMCM22 sample

The XRD patterns were in good agreement with those reported in the literature [27], and no other X-ray lines due to impurities were present. SEM showed that the sample comprised mainly platelets with a thickness of approximately 0.1 μm and sizes between 1 μm × 0.7 μm and 2 μm × 1.4 μm, associated into particles.

The main physicochemical characteristics of the sample (Si/Al = 14.5) are presented in Table 1: micropore volume and external surface area obtained from nitrogen adsorption; total concentrations of Brønsted and Lewis acid sites, determined from the intensities of the bands at 1545 (pyridinium ions, PyH^+) and 1455 cm^{-1} (pyridine coordinated to Lewis sites, Py-L); concentration of the external Brønsted sites estimated by 2,4-DMQ adsorption followed by IR spectroscopy; relative distribution of the bridging OH groups estimated by deconvolution of the band at 3620 cm^{-1} into three bands, which, according to Onida et al. [35], correspond to OH groups located in supercages (3628 cm^{-1}), sinusoidal channels (3618 cm^{-1}), and hexagonal prisms (3585 cm^{-1}).

The values given in Table 1 show that the material has a micropore volume of ∼0.2 cm^3 g^{-1} and an external surface area of ∼91 m^2 g^{-1}. This includes the surface of interparticle mesopores, because a steep rise of the isotherm at $p/p^o < 1$ indicated capillary condensation in mesopores. The difference between the uptake (expressed in terms of liquid volume) estimated at $p/p^o = 0.97$ and the micropore volume will be used to probe any eventual alterations in the mesopores.

Fig. 1a represents the IR spectra of HMCM-22 in the OH-stretching region (3800–3500 cm^{-1}) before and after pyridine adsorption at 150 °C and then pyridine desorption between 150 and 500 °C. In agreement with previous works [24,27,35,36], four hydroxyl bands are seen. The main one at 3620 cm^{-1}, with a shoulder at 3580 cm^{-1}, corresponds to bridged hydroxyl groups (Al–OH–Si); the band at 3670 cm^{-1} often is ascribed to hydroxyl groups linked to extra-framework aluminium species (probably generated during calcination treatments); and the bands at 3730 and 3747 cm^{-1} are ascribed to internal and external silanol groups, respectively. Pyridine adsorption (then evacuation) at 150 °C had practically no effect on the band at 3730 cm^{-1}, but caused the complete disappearance of the band at 3620 cm^{-1} and a decrease

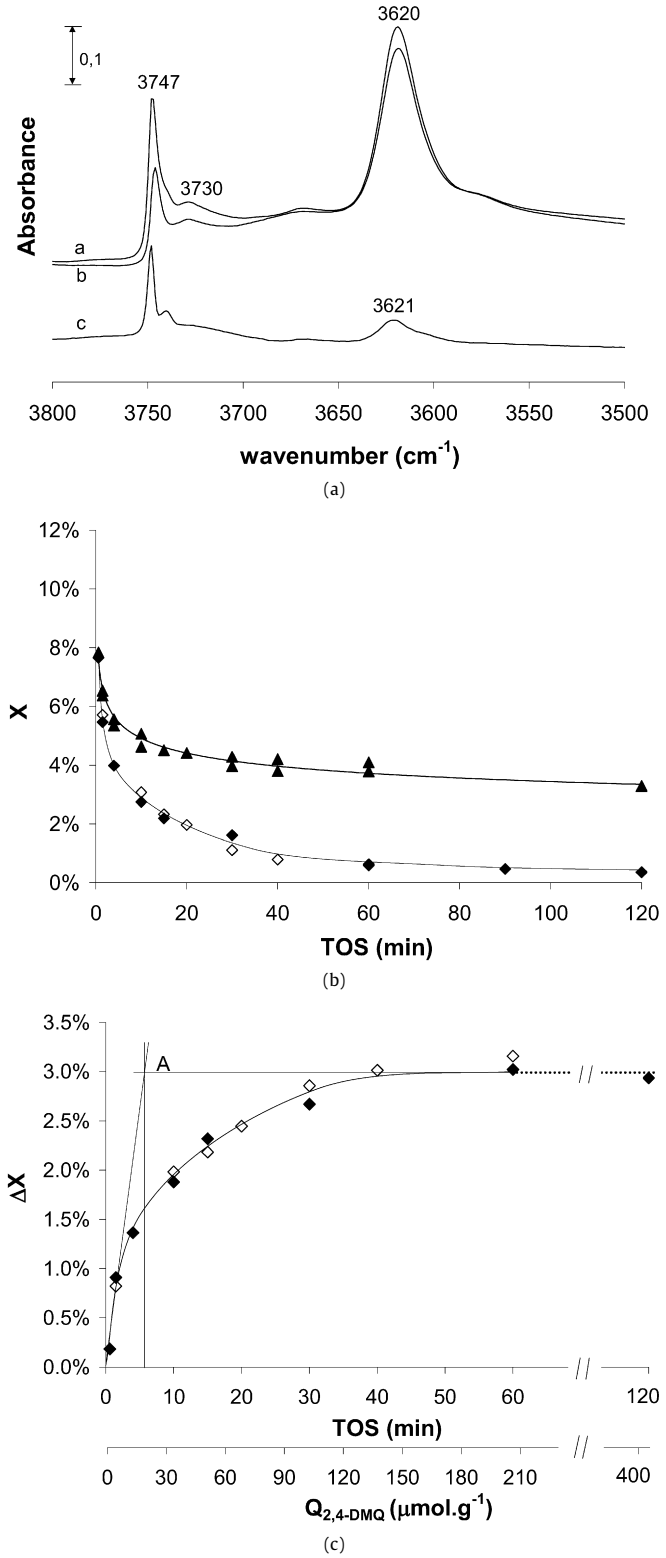

Fig. 2. (a) IR spectra of the hydroxyl region of the HMCM-22 sample before (a), after 2,4-DMQ adsorption (b) and (c) difference spectrum (a–b); (b) transformation of methylcyclohexane on HMCM-22 as a function of time-on-stream (TOS) in (▲) absence and in (◇,◆) presence of 2,4-DMQ; (c) decrease in methylcyclohexane conversion (ΔX) as a function of TOS and of the amount of 2,4-DMQ injected on the catalyst.

in the intensity of the bands at 3670 and 3747 cm^{-1} (Fig. 1a). The band at 3620 cm^{-1} began to reappear after desorption at 350 °C, but only ∼65% of the intensity was recovered after desorption of pyridine at 500 °C, which suggests that these bridged OH groups are strongly acidic. This strong protonic acidity is confirmed by the persistence of the PyH^+ band at 1545 cm^{-1} (∼20% of the value after desorption at 500 °C). It should be noted that, in agreement with the literature, the Py-L band at 1455 cm^{-1} was not affected by desorption at 500 °C, suggesting that Lewis sites are stronger than Brønsted sites.

The distribution of the bridging hydroxyl groups among supercages, sinusoidal channels, and hexagonal prisms can be estimated by deconvolution [35] of the band resulting from the difference between IR spectra before pyridine adsorption and after desorption at 150 °C (Fig. 1b). Good agreement was obtained between experimental (continuous line) and calculated (dotted line) curves representing the total area of the OH band. The semi-quantitative distribution estimated by considering the extinction coefficients as identical: ∼70% in supercages, ∼20% in sinusoidal channels, and ∼10% in hexagonal prisms was not very different from those reported previously (e.g., 54, 33, and 14% [35]; 60–70, 19–29, and 6% [36]; 60, 22–24, and 16–18% [23]).

The concentration of protonic sites located in the external cups was estimated as described previously: adsorption of a bulky basic molecule (2,4-dimethylquinoline [2,4-DMQ]), followed by IR spectroscopy [33] and poisoning of methylcyclohexane transformation by the same basic molecule [22,23]. As was demonstrated previously [33], owing to the long contact time of 2,4-DMQ molecules with the zeolite during the IR experiments, protonation can occur not only on the protonic sites of the external pockets, but also on part of the inner sites. The protonation of these latter sites causes a decrease in the intensity of the bridging OH band at 3620 cm^{-1} (Fig. 2a); therefore, the concentration of the external sites can be estimated by the difference between the total concentration of 2,4-DMQ^+ ions calculated from the intensity of the band at 1645 cm^{-1} and the concentration of the inner bridging OH groups adsorbing 2,4-DMQ molecules deduced from the difference of the intensity of this band before and after 2,4-DMQ adsorption. This concentration was found to be equal to ∼25 μmol g^{-1}.

Fig. 2b plots the curves giving the decrease in methylcyclohexane conversion (X) versus time on stream (TOS) in the absence and in presence of 2,4-DMQ (two different experiments). In both cases, an initial decrease in conversion is followed by a quasi-plateau for TOS > 40 min, with the decrease more pronounced in the presence of 2,4-DMQ. The difference between X in the absence and the presence of 2,4-DMQ (ΔX) corresponds to the poisoning effect of 2,4-DMQ (Fig. 2c). By assuming that at short TOS values, all of the 2,4-DMQ molecules have a poisoning effect, the values of TOS and of the amount of 2,4-DMQ needed to obtain the maximum deactivation (Q) are given by point A. As was found with *m*-xylene transformation on various MCM22 samples [33], the Q value (20–25 μmol g^{-1}) is very close to the concentration of external protonic sites estimated by 2,4-DMQ adsorption (Table 1). This is a strong argument in favour of the validity of both methods of determining the external protonic acidity.

3.2. Methylcyclohexane transformation

As has been observed with other reactions, including *n*-heptane cracking [37], xylene isomerisation [25], toluene disproportionation [7,9], butene isomerisation [38], and others, a very fast initial deactivation occurred, followed by a quasi-plateau of activity (Fig. 3). Thus, for a contact time τ (taken here as the reverse of the WHSV) of 0.065 h, the conversion of methylcyclohexane (mch) X passed from ∼8% at 0.6 min to ∼4.6% for TOS = 10 min, and then to 4.1% for TOS = 60 min and to 1.5% for TOS = 600 min. Fig. 4 suggests that catalyst deactivation is due to carbonaceous deposits (coke). Indeed, the plot of the percentage of coke versus

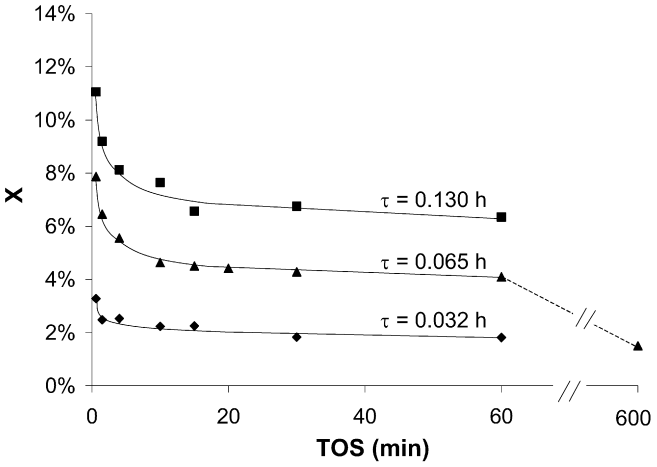

Fig. 3. Influence of time-on-stream (TOS) on methylcyclohexane conversion X (%) for three values of contact time (τ).

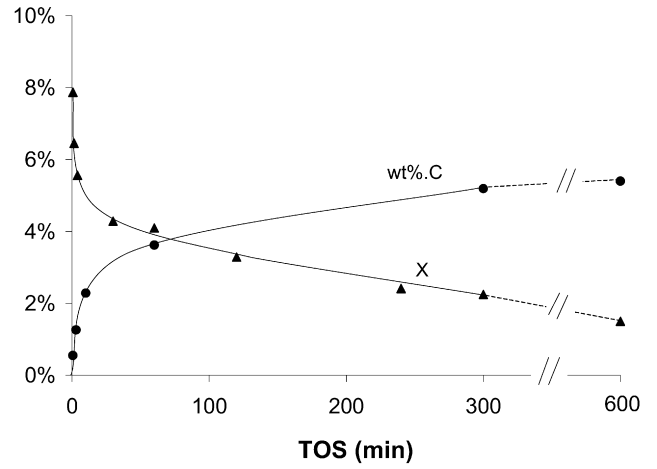

Fig. 4. Influence of time-on-stream (TOS) on methylcyclohexane conversion X (%) and on the percentage of coke deposited on the zeolite (wt% C) at 350 °C for a contact time of 0.065 h.

TOS for $\tau = 0.065$ h is symmetrical to the deactivation curve: very fast initial formation of coke, followed by a much more progressive increase. The initial (TOS = 0.6 min) mch conversion to coke was 3.6%, only 2.2 times lower than the conversion into desorbed products. For TOS = 60 min, the conversion into coke was 0.09%, ~40 times lower than the conversion to desorbed products.

3.2.1. Reaction rates

The desorbed reaction products can be classified into three main families: dimethyl and ethylcyclopentane isomers of methylcyclohexane (I), C_2–C_8 aliphatic alkanes and alkenes (with also a tiny amount of methane) (C), and benzenic hydrocarbons (A). As shown in Fig. 5a, on the fresh catalyst, the I, C, and A products seemed to result directly from mch transformation; that is, these are apparent primary products. However, the selectivity to C products increased with the mch conversion rate (X) at the expense of the selectivity to isomers I, suggesting a secondary mode of formation of the C from I products (Fig. 5b). Furthermore, TOS had practically no effect on the I, C, and A distribution: 52–55 wt% of I, 36–41 wt% of C, and 4–8 wt% of A products.

The total activity of the catalyst, both fresh and after 60 and 600 min of reaction, was estimated from the slope of the tangent at contact time $\tau = 0$ to the curves giving the conversion rate X versus τ (Fig. 5a). Furthermore, the activities in the formation of each product family, I, C, and A, were drawn from the total activity values and from the product distribution at zero conversion drawn from Fig. 5b, and the coking activity was deduced from the effect of TOS on coke content (Fig. 4). Table 2 shows that deactivation affected the formation of all of the desorbed products similarly (in agreement with the negligible effect of TOS on product distribution shown below) and had a much more pronounced effect on coke formation.

3.2.2. Product distribution

Table 3 presents the detailed distribution of the products formed over the fresh and deactivated catalysts for various values of τ, and thus of X. The initial product distribution over the fresh catalyst, obtained by extrapolation at zero conversion, is reported in the first column. This initial product distribution, which is similar to that found at 350 °C over a large-pore FAU zeolite (HUSY) [39], was as expected from a classical carbenium ion chain mechanism. In agreement with this mechanism, no methane (actually only traces) was produced; isomers (I), C_3–C_7 aliphatic products (C), and aromatics (A) appeared as primary products; the C_4–C_7 products were mainly branched; and the value of the olefin/paraffin ratio in the C products was very low (0.18), indicating a high rate of hydrogen transfer (HT) steps. Indeed, the cracking of one molecule of methylcyclohexane occurred through two successive steps: formation of one molecule of heptene, followed by cracking of this olefin into two olefins, resulting in an olefin/paraffin ratio equal to ∞. Furthermore, the near absence of heptenes in the C products (and the low amount of heptanes produced by HT—only 0.3 wt%) (Table 3) demonstrates that the second step of cracking was much faster than the first step. As expected, the more facile the HT steps, the lower the olefin/paraffin ratio. Thus this ratio was equal to ∞ in the C_2 products for which HT would involve ethyl carbenium ions as transition states, to 0.27 and 0.37 in the C_3 and nC_4 (secondary carbenium ions), and to 0 in the iC_4 and C_5–C_7 products, which are mainly branched (tertiary carbenium ions).

But the composition of the C products cannot be explained by cracking and hydrogen steps only. Indeed, the C_2/C_5 and C_3/C_4 molar ratios were <1 (0.8 and 0.6, respectively) and formation of C_6 occurred without formation of methane. This indicates that after methylcyclohexane cracking, not only HT steps (which are known to be very fast), but also a complete reorganisation of the cracking product distribution through an alkylation-cracking process occurred before product desorption.

Likewise, the mixture of toluene and xylenes (essentially *meta*- and *para*-isomers) that constitutes the A products could not result from the most expected process—HT from methylcyclohexane to olefinic cracking products with toluene formation [Eq. (1)], followed by disproportionation into benzene and xylenes [Eq. (2)]:

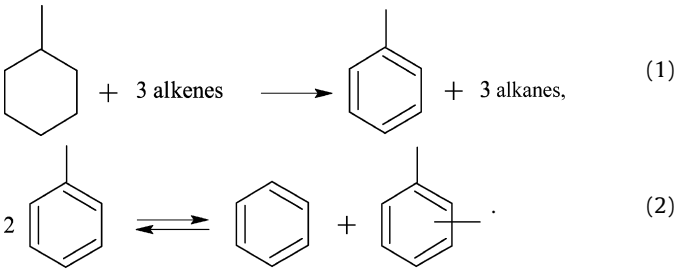

Indeed, no benzene was observed, suggesting that xylenes and probably some toluene resulted from another reaction, most likely aromatisation of the cracking products. Another important observation is that the molar alkane/benzenic ratio was much greater than 3 (i.e., 13.4), which is the value expected from methylcyclohexane transformation into toluene [Eq. (1)]. This means that over the fresh catalyst, most of the hydrogen atoms responsible for olefin saturation (~80%) originated from coke precursors.

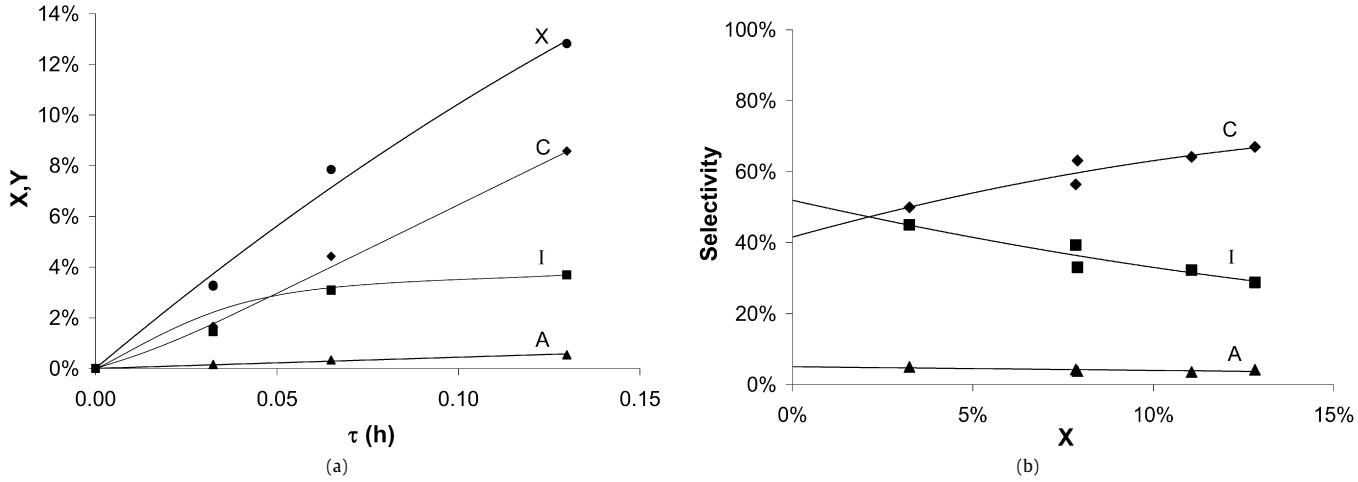

Fig. 5. Methylcyclohexane transformation over the fresh HMCM-22 sample: (a) influence of contact time τ on methylcyclohexane conversion X and on the yields Y (wt%) in cracking (C), isomers (I) and aromatic (A) products and (b) influence of methylcyclohexane conversion (X) on the selectivity (wt%) to C, I and A products.

Table 2
Influence of time-on-stream (TOS) on the activity (mmol h^{-1} g^{-1}) of the HMCM22 sample for methylcyclohexane transformation (total) and for isomerisation (I), cracking (C), aromatic (A) and coke products. Relative activity values (fresh catalyst TOS = 0.6 min as reference) are given between brackets

Activity	Total	Isomerisation	Cracking	Aromatisation	Coking
TOS = 0.6 min	12.3 (1)	6.6 (1)	5.1 (1)	0.6 (1)	5.7 (1)
TOS = 60 min	6.3 (0.51)	3.4 (0.51)	2.4 (0.47)	0.5 (0.83)	0.13 (0.02)
TOS = 600 min	2.3 (0.19)	1.3 (0.2)	0.9 (0.18)	0.14 (0.18)	0.002 (0.00035)

Table 3
Methylcyclohexane transformation

	Fresh catalyst				TOS 60 min			TOS 600 min
τ (h)	0[a]	0.032	0.065	0.13	0.032	0.065	0.13	0.065
X (%)	0[a]	3.3	7.8	11.0	1.8	4.1	7.45	1.5
Ethylene	2.1	1.8	1.5	1.2	0.6	0.45	0.4	0.5
Propane	7.0	8.2	7.6	9.3	3.5	3.0	2.5	2.5
Propylene	1.9	1.5	0.8	0.6	2.6	1.45	1.4	2.8
Butanes	19.7	23.4	26.1	32.3	12.6	8.6	7.2	7.6
Butenes	0.7	0.6	0.5	0.4	0.8	0.46	0.35	1.2
Pentanes + pentenes	6.5	7.7	11.2	13	4.7	3.7	3.3	3.9
Hexanes	5.9	7.0	7.5	6.2	8.6	8.9	6.4	5.4
Hexenes	0	0	0.05	0.1	0	0.25	0.3	0.6
Heptanes	0.3	0.2	0.2	0.2	4.4	1.66	2.1	6.6
Heptenes	0	0	0.09	0.07	1.5	2.35	1.8	1.3
Octanes	0	0	0.74	0.8	2.8	6.7	6.6	5.5
Isomers	50.2	44.6	39.4	32.3	48.7	51.6	53.2	56.3
Benzene	0	0	0	0	0	0.16	0.35	1.3
Toluene	2.3	1.8	1.61	1.3	4.2	3.9	4.5	2.4
$(m+p)$-Xylene	3.4	3.2	2.5	2.0	4.4	4.6	5.6	2.1
o-Xylene	0	0	0.2	0.2	0.6	0.7	1	0
Trimethylbenzene	0	0	0	0	0	1.5	3	0
Total	100	100	100	100	100	100	100	100
Distribution (wt%)								
Isomers (I)	50.2	44.6	39.4	32.3	48.7	51.6	53.2	56.3
Cracking (C)	44.1	50.4	56.3	64.2	42.1	37.5	32.4	37.9
Aromatics (A)	5.7	5.0	4.3	3.5	9.2	10.9	14.4	5.8
Molar ratios								
iC_4/nC_4	7.8	7.6	7.1	7.0	7.2	8.7	9.9	5.7
C_3/C_4	0.6	0.5	0.4	0.4	0.6	0.65	0.7	0.8
C_2/C_5	0.8	0.6	0.3	0.2	0.3	0.3	0.3	0.3
Alkenes/alkanes	0.18	0.14	0.09	0.06	0.2	0.18	0.2	0.3
Alkanes/benzenics	13.4	17.6	22.7	32.0	6.3	4.5	2.8	7.5

Product distribution (wt%) over the fresh sample and after 60 and 600 min reaction.
[a] Values of the initial distribution obtained by extrapolation at zero conversion.

The main reactions involved in mch transformations—isomerisation (I), cracking (C), dimerisation-cracking (D–C), hydrogen transfer (HT), aromatisation (Ar), and coke formation—are presented in Scheme 1:

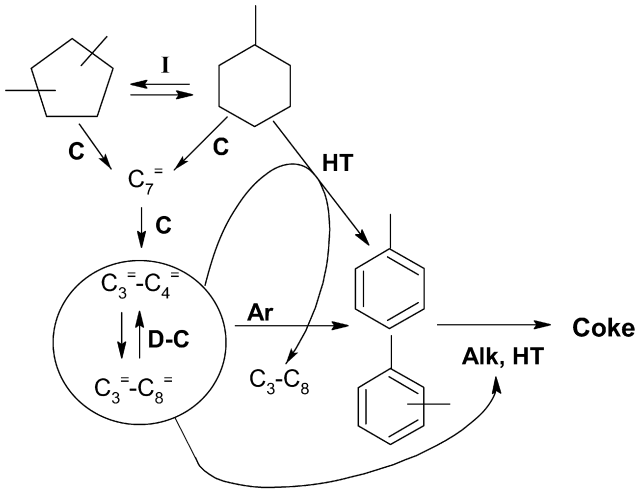

Scheme 1. Main transformations of methylcyclohexane over the HMCM-22 zeolite: I: isomerisation, C: cracking, D–C: dimerisation–cracking, HT: hydrogen transfer, Ar: aromatisation, Alk: alkylation.

The product distribution was affected by the conversion rate (X), decreased selectivity to isomers to the benefit of C products and increased significance of secondary transformations of the cracking products, lower values of the molar C_2/C_5 and C_3/C_4 ratios, and lower values of the olefin/paraffin ratio (Table 3, columns 1–4), due to greater significance of the alkylation cracking and hydrogen transfer steps. An increase with X of the alkane/benzenic ratio, and thus of the selectivity to coke, also can be observed.

TOS affected the product distribution. Thus, for similar values of X (e.g., 3–4% over the fresh and 1-h deactivated samples or 1.8–1.5 on the samples deactivated for 60 and 600 min, Table 3), increases in the percentages of I and A products occurred with increasing TOS at the expense of the C products. But the main effect of TOS was on the distribution of the C and A products; for similar X values (Table 4), significant increases in the percentages of C_6–C_8 aliphatic products occurred with increasing TOS at the expense of the C_3–C_4 products. For X values of 3–4% (columns 1 and 2, Table 4), at TOS = 60 min, the percentage of C_6–C_8 products in the C products increased from 14 wt% on the fresh sample to 53 wt%, whereas the that of C_3–C_4 products decreased from ~67 to 36 wt%. Another important change was the decrease in the alkane/aromatic molar ratio from 18 to 4.5 (Table 3, columns 1 and 6). The formation of large amounts of C_7 products (heptanes and heptenes) means that some of the heptenes resulting from scission of mch and isomers (Scheme 1) no longer underwent secondary cracking into C_3–C_4 products. Furthermore, the appearance of C_8 products (essentially octanes) confirms the decrease in cracking reactions. With increasing TOS, the distribution of the benzenic products (A) passed progressively from that ascribed to an aromatisation process, particularly with formation of xylenes but not of benzene, to that expected of a hydrogen transfer-disproportionation process [Eqs. (1) and (2)] at TOS = 600 min, with a benzene/xylene molar ratio close to 1. This indicates that deactivation inhibited several reactions, including cracking of C_7–C_8 intermediates and aromatisation.

3.3. Composition of coke and effect on acidity and porosity

The main IR bands typical of the carbonaceous deposits (1300–1700 cm^{-1} region) are shown in Fig. 6 for the coked samples corresponding to the experiments of Fig. 4. The spectra are quite similar to those obtained on HMWW samples coked during *m*-xylene (mX) transformation at 350 °C and ascribed to methyl polyaromatic compounds [24]. As can be seen, the integrated absorbances of the bands are proportional to the amount of coke deposited on the zeolite.

The composition of coke was qualitatively established for samples b, c and e characterised by IR spectroscopy (Fig. 6), which contained 2.3, 3.6, and 5.4 wt% coke, respectively. With samples b and c, all of the carbonaceous compounds were found to be soluble in methylene chloride after dissolution of the zeolite in hydrofluoric acid. With sample e, a very small amount of insoluble compounds appeared in the form of black particles, which could not be recovered. Furthermore, no carbonaceous compounds could be recovered through a direct Soxhlet treatment of the coked samples, demonstrating that all of the coke components were trapped inside the zeolite pores.

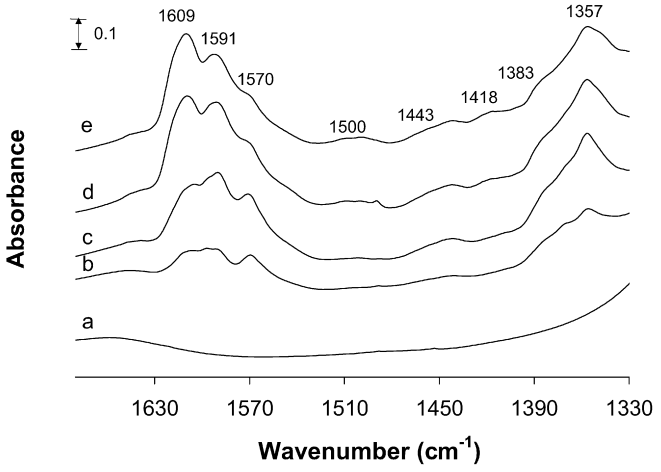

Fig. 6. 1300–1700 cm^{-1} region of the IR spectra of the samples coked during methylcyclohexane transformation at 350 °C for various time-on-stream (TOS): (a) 0 min (fresh), (b) 10 min (2.3 wt% C), (c) 60 min (3.6 wt% C), (d) 300 min (5.2 wt% C) and (e) 600 min (5.4 wt% C).

Table 4
Distribution of the C products (wt%) for similar values of conversion rate (X) and different values of time-on-stream (TOS)

TOS (min)	0.6	60	60	600
X (%)	3.3 ($\tau = 0.032$ h)	4.1 ($\tau = 0.065$ h)	1.8 ($\tau = 0.032$ h)	1.5 ($\tau = 0.065$ h)
C_2	3.7	1.2	1.4	1.2
C_3	19.2	11.8	14.4	13.9
C_4	47.5	24.2	32.2	23.5
C_5	15.3	9.9	11.1	10.2
C_6	13.9	24.4	20.4	15.8
C_7	0.4	10.6	13.9	20.9
C_8	3.7	17.9	6.6	14.5

With samples b and c (TOS of 10 and 60 min, respectively), the main coke components were methyl naphthalenes, accompanied by traces of methylphenanthrenes and methylpyrenes. The coke of sample e (TOS = 600 min) contained essentially methyl binaphthyles and small amounts of methyl pyrene and methylfluoranthene compounds. It should be noted that the coke components were not exactly those formed during mX transformation. The main difference is the presence in this latter coke of trimethylbenzenes and tetramethylbenzenes, which were not observed here, and the absence of methyl binaphthyles. These differences likely result from the significant differences in the composition of the reaction mixtures, especially in the relative amounts of the coke precursor molecules, that is, aromatics and olefins [40]. From mX, the reaction mixture contained essentially xylenes and trace amounts of C_2–C_4 olefins, from mch essentially light olefins with small amounts of toluene and xylenes.

Scheme 2 can be proposed for coke formation from mch. The primary products of mch transformation (Scheme 1) contained large amounts of light olefins, which are well-known coke-making molecules [40]. Therefore, methyl naphthalenes, the first observed coke molecules, may have essentially resulted from transformation of light olefinic products. These primary products aromatised into toluene and xylenes and alkylated these benzenic compounds. The alkylate products may have led, through several successive intramolecular (cyclisation, isomerisation) and intermolecular (HT to the olefinic products) reactions, to methylnaphthalenes. Through the same route, methylnaphthalenes could be transformed into heavier polyaromatics, such as methyl pyrenes; however, this route was not predominant, probably because methylnaphthalene molecules formed in large amounts within the pores in which they were trapped inhibited the chemisorption of the less basic light olefins. Consequently, essentially reactions of condensation of methylnaphthalene molecules could occur with formation of methylbinaphthyles.

As was the case for coke molecules formed in mX transformation, the coke molecules most likely were formed and trapped within the supercages. Indeed, as indicated above, no carbonaceous compounds could be recovered by direct Soxhlet treatment of the coked zeolite; thus, coke could not be located in the external cups. Furthermore, most of the bimolecular intermediates involved in many steps of coke formation and most of the coke molecules were too bulky to be accommodated at the intersection of the sinusoidal channels. Due to their large size (diameter, 7.1 Å; height, 18.2 Å) and the small size of their apertures (4.0 × 5.5 Å), the supercages easily trapped the coke molecules, explaining the high initial rate of coking.

Other arguments in favour of the trapping of coke molecules within the supercages can be drawn from the effect of coke on the accessible micropore volume and acidity, which was determined with the samples shown in Fig. 6. Fig. 7 shows that coke caused a significant decrease in the micropore volume accessible to nitrogen but had practically no effect on the volume of interparticle mesopores; however, after 600 min of reaction (sample e, coke content of 5.4 wt%), ~40% of the micropore volume remained accessible. With *p*-xylene as an adsorbate (Fig. 8), a lower value (~30%) was found, meaning that coke made ~70% of the micropore volume inaccessible. These latter values are in good agreement with the relative volume of sinusoidal channels and supercages estimated by molecular modelling simulation: ~30% and 70% of the micropore volume, respectively [41]. Furthermore, a comparison plot of the two isotherms (inset of Fig. 8) shows linear results with a slope close to 1, indicating (also using this adsorptive) that no significant changes occurred on the external surface, including mesopores.

The IR spectra shown in Fig. 9 indicate that coke had a significant effect on the intensity of the bridging OH bands that

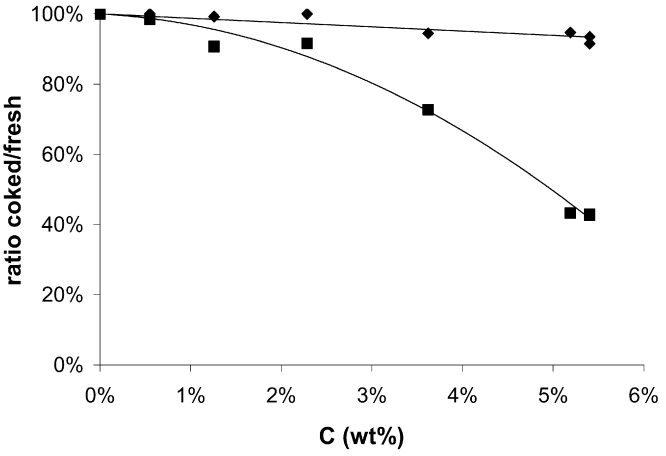

Fig. 7. Influence of coke on the residual (ratio between values for coked and fresh catalyst) micropore volume (■) and mesopore volume (◆) (taken here as the difference between the total pore volume *V* (0.97) and the micropore volume).

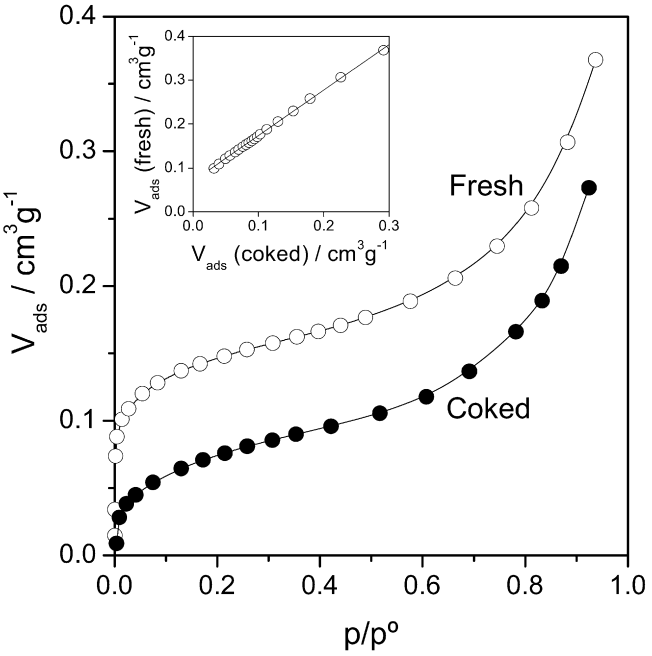

Fig. 8. Adsorption isotherms of *p*-xylene determined, at 298 K, on fresh HMCM22 and after 600 min reaction (coke content of 5.4 wt%). (The inset shows the comparison of adsorption data obtained on fresh sample towards that of coked.)

correspond to the inner protonic acid sites of the zeolite. With sample e (wt% coke of 5.4), the intensity of the band at 3620 cm^{-1} was 40% of that corresponding to the fresh sample a. Deconvolution of this band showed that this decrease was due mainly to the OH groups located in the supercages. The concentrations of Brønsted and Lewis sites also were estimated by pyridine adsorption at 150 °C, followed by IR spectroscopy. Fig. 10 shows that the effect of coke was less pronounced on the concentration of protonic sites estimated from the intensity of the pyridinium band at 1545 cm^{-1} (curve PyH^+) than on the absorbance of the bridging OH band (curve OH). The difference was more pronounced at low coke content than at high coke content. Similar observations were previously made, first with USHY samples coked during *m*-xylene transformation [42] and then with other zeolites, including the MWW zeolite [24]. The lesser effect of coke on the concentration of protonic sites was demonstrated to be due to desorption of

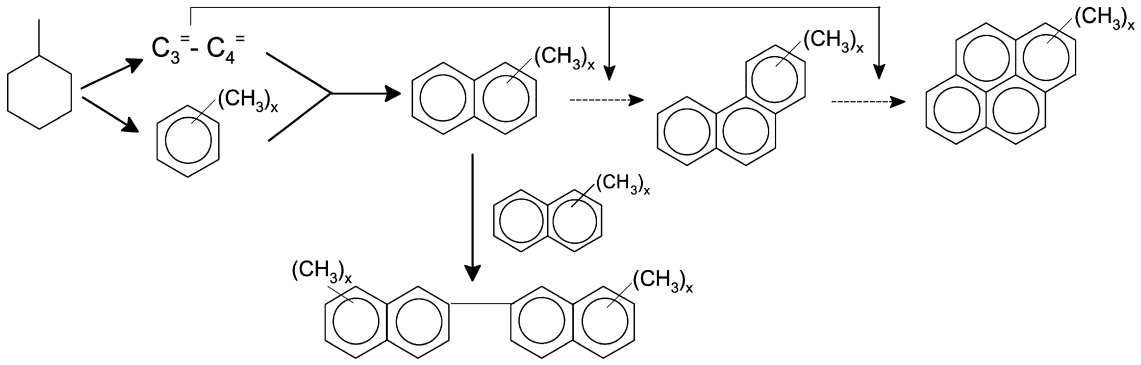

Scheme 2. Mode of coke formation from methylcyclohexane.

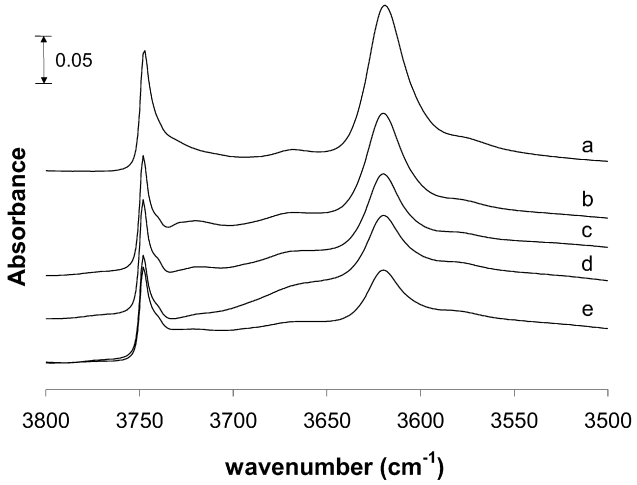

Fig. 9. Influence of coke on the OH-stretching region of IR spectra of HMCM-22 samples: (a) fresh (0 min), (b) 10 min (2.3 wt% C), (c) 60 min (3.6 wt% C), (d) 300 min (5.2 wt% C) and (e) 600 min (5.4 wt% C).

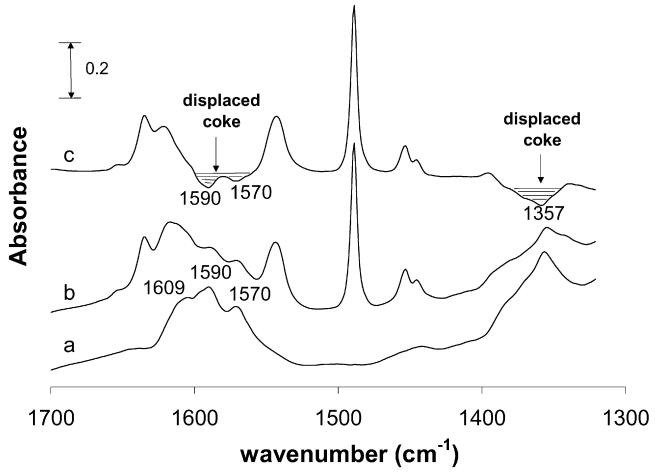

Fig. 11. Influence of pyridine adsorption at 150 °C on the intensity of the bands of coke (1700–1300 cm^{-1}) over the MCM-22 samples coked for 60 min (3.6 wt% C), (a) before and (b) after pyridine adsorption, (c) difference spectrum (a–b).

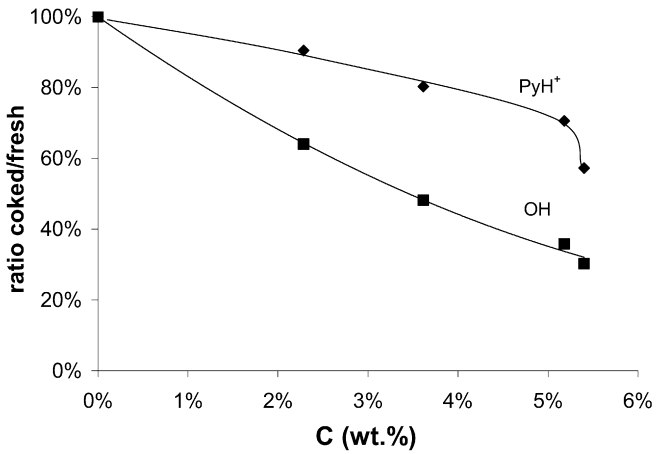

Fig. 10. Influence of coke on the relative values (coked/fresh) of the integrated surface of PyH^+ (◆) band and of the bridging OH band (■).

some of the coke molecules by the more basic pyridine molecules [42]. This explanation was confirmed in the present work. Indeed, with all of the coked samples, and especially at low coke content, pyridine adsorption caused a significant decrease of the bands at 1357, 1570, and 1590–1610 cm^{-1}. This is clearly shown on the difference spectrum in Fig. 11 for sample c (TOS = 60 min, coke content of 3.6 wt%). Therefore, it is not possible to estimate the concentration of the protonic sites not deactivated by coke from the classical method based on the intensity of pyridinium bands; however, a qualitative estimation can be made from the area of the bridged OH band (OH curve, Fig. 10); from this curve, by supposing similar values of the extinction coefficients for the three types of OH (in supercages, sinusoidal channels, and hexagonal prisms), it can be concluded that for sample e (TOS = 600 min, 5.4 wt% coke), ∼30% of the bridged OH groups did not interact with coke molecules, roughly corresponding to the sum of the percentages of sites located in the sinusoidal channels and hexagonal prisms. This is an additional argument in favour of the formation of coke within the supercages only.

An atypical evolution with coke content was found for the band corresponding to pyridine adsorbed on the Lewis sites (PyL). At low coke content (i.e., short TOS), the concentration of Lewis sites increased from 128 to 195 $\mu mol\,g^{-1}$, up to 2.3 wt% of coke (i.e., TOS = 10 min), followed by a decrease in these sites to close to the initial value. This unexpected initial increase was previously observed with USHY zeolite [43] and can be tentatively ascribed to a change in the extinction coefficient.

3.4. Catalytic role of the three-pore systems

We applied the method developed for determining the catalytic role of the three-pore systems in xylene transformation [22]. This method involves two main steps:

a) Selective and complete deactivation of the supercage sites, which can be carried out by coke deposition during *m*-xylene transformation at 350 °C for a long period (i.e., 10 h). In this work, catalytic measurements and bridging OH groups infrared

Table 5
Determination of the product yield (wt%) for methylcyclohexane transformation within the supercages by difference between the yields obtained with the fresh sample and with the sample aged for 10 h during *m*-xylene (or methylcyclohexane) transformation and product distribution (wt%) (values in brackets)

τ (h)	0.065			0.13		
	Fresh	Aged	Supercages	Fresh	Aged	Supercages
X (%)	7.84	1.45	6.39	11.04	1.86	9.18
Ethylene	0.114	0.01	0.1 (1.6)	0.13	0.02	0.11 (1.2)
Propane	0.6	0.075	0.52 (8.1)	1.03	0.15	0.88 (9.5)
Propylene	0.066	0.033	0.033 (0.5)	0.07	0.07	0 (0)
Butanes	2.05	0.163	1.89 (29.4)	3.56	0.25	3.31 (35.6)
Butenes	0.037	0.02	0.017 (0.26)	0.044	0.048	**−0.004**
Pentanes	0.88	0.06	0.82 (12.7)	1.44	0.09	1.35 (14.5)
Pentenes	0.0	0.01	**−0.01**	0	**0.013**	**−0.013**
Hexanes	0.59	0.088	0.5 (7.8)	0.69	0.12	0.57 (6.1)
Hexenes	0.004	0.01	**−0.006**	0	0.017	**−0.017**
Heptanes	0.014	0.028	**−0.014**	0.01	0.046	**−0.036**
Heptenes	0.007	0.014	**−0.007**	0.008	0.035	**−0.027**
Octanes	0.058	0.065	**−0.007**	0.093	0.029	0.064 (0.7)
Isomers	3.09	0.785	2.3 (35.7)	3.56	0.84	2.72 (29.3)
Benzene	0	0.008	**−0.01**	0	0.018	**−0.018**
Toluene	0.126	0.035	0.09 (1.4)	0.15	0.062	0.09 (1.0)
$(m+p)$-Xylene	0.195	0.042	0.15 (2.35)	0.22	0.045	0.175 (1.9)
o-Xylene	0.013	0	0.013 (0.2)	0.022	0	0.022 (0.2)
Total	7.84	1.45	6.44	11.04	1.86	9.30
Distribution (wt%)						
Isomers (I)	39.4	54.1	35.7	32.4	45.1	29.3
Cracking (C)	56.3	39.9	60.3	64.0	48.2	67.6
Aromatics (A)	4.3	6.0	4.0	3.6	6.7	3.1
Molar ratios						
iC_4/nC_4	7.1	4.9	7.4	7.0	3.4	7.6
C_3/C_4	0.4	0.8	0.4	0.4	1.0	0.36
C_2/C_5	0.3	0.4	0.3	0.2	0.5	0.2
Alkenes/alkanes	0.09	0.2	0.06	0.06	0.33	0.03
Alkanes/benzenics	22.7	8.3	33.2	32.0	9.8	33.5

spectroscopy confirmed that 10 h of ageing was sufficient to completely deactivate the protonic sites of supercages; no further deactivation or no decrease in the bridging OH band was observed. Because the active sites of the external cups and of the sinusoidal channels were not affected, the mch conversion rate (X) and the product yields in the supercages are given by the differences between those obtained on the fresh and on the *m*-xylene-deactivated samples. Furthermore, the values obtained on the *m*-xylene-deactivated sample corresponded to methylcyclohexane transformation in the other pore systems (external cups and sinusoidal channels).

b) Selective and complete poisoning of the protonic sites of the external cups with 2,4-dimethylquinoline (2,4-DMQ), a basic molecule too bulky for entering the inner micropores. When this poisoning is applied on the MCM22 sample deactivated during *m*-xylene transformation for 10 h, the residual activity corresponds to that of the sinusoidal channels.
Deactivation by coke formed during *m*-xylene transformation for 10 h and poisoning with 2,4-DMQ added to the mch reactant were successively carried out on MCM22 samples for three values of contact times τ: 0.032, 0.065, and 0.13 h.

3.4.1. Catalytic role of supercages

The yields in the main products obtained over the fresh and *m*-xylene-deactivated MCM22 zeolite, as well as their difference (which should be due to mch transformation in the supercages) are reported in Table 5 for two values of contact time τ: 0.065 and 0.13 h. Three remarks can be made:

a) The mch conversion (X) and the corresponding product distributions obtained after *m*-xylene (mX) and mch transformation for 10 h were quite similar (see the last column in Table 3 and column 2 in Table 5). This means that coke deposited from both reactants had the same effect, causing complete deactivation of the supercage active sites. After that, the catalyst was very stable, suggesting that mch transformation occurred within the sinusoidal channels and the external pockets with no deactivation.

b) Supercages played a predominant role in methylcyclohexane transformation over the fresh HMCM22 sample: more than 80% of the mch transformation into desorbed products occurred in the supercages.

c) For τ equal to 0.065 and 0.13 h (Table 5), and also for $\tau =$ 0.032 h (data not reported), negative values of yields were obtained for pentenes, hexenes, heptanes and heptenes and probably for C_8 and benzene. Table 5 shows that the main parts of these products appeared after deactivation. A likely explanation for this is that these products were formed on the protonic sites of the sinusoidal channels or/and of the external cups and that they were rapidly transformed on the supercage sites on the fresh catalyst. At least for alkene products, this suggestion is in good agreement with their high reactivity.

Consequently, the distribution of the desorbed products resulting from the direct mch transformation in the supercages can be estimated by considering only the products with positive yield values. This distribution is reported into brackets in columns 3 (contact time $\tau = 0.065$ h) and 6 ($\tau = 0.13$ h). Because most of mch transformation over the HMCM22 sample occurred within the supercages, the supercage product distribution (Table 5) was close to the total distribution (Table 3) and also close to that found over a USHY zeolite. Therefore, Scheme 1, in which reactions occur through the carbenium ion chain mechanism, can account for the mode of mch transformation within the large supercages of MCM22 and FAU zeolites, despite the difference in aperture size.

Table 6
Yields (wt%) in products formed within the Sinusoidal Channels (S.C.), values obtained on the sample aged for 10 h with *m*-xylene then poisoned with 2,4-DMQ (2) and within the external cups (Ext.): difference between the yields of the aged sample and those obtained for the sinusoidal channels (3 = 1–2); Product distribution (wt%): values in brackets

τ (h)	0.065			0.13		
	1) S.C. + Ext.	2) S.C.	3) Ext	1) S.C. + Ext.	2) S.C.	3) Ext
X (%)	1.45	0.17	1.28	1.86	0.35	1.51
Methane	0.003	0.002 (1.1)	0.001 (0.08)	0.009	0.007 (2)	0.002 (0.16)
Ethylene	0.01	0.003 (1.9)	0.007 (0.51)	0.02	0.008 (2.3)	0.012 (0.83)
Propane	0.075	0.016 (9.4)	0.059 (4.6)	0.15	0.047 (13.4)	0.1 (6.8)
Propylene	0.033	0.009 (5.7)	0.024 (1.8)	0.07	0.027 (7.9)	0.04 (2.9)
Butanes	0.163	0.015 (8.7)	0.148 (11.6)	0.25	0.042 (12.1)	0.21 (13.8)
Butenes	0.02	0.015 (8.9)	0.005 (0.45)	0.048	0.036 (10.3)	0.012 (0.8)
Pentanes	0.06	0.004 (2.5)	0.056 (4.35)	0.09	0.01 (3.2)	0.08 (5.3)
Pentenes	0.01	0.002 (0.9)	0.006 (0.5)	0.013	0.008 (2.4)	0.005 (0.3)
Hexanes	0.088	0.002 (1.2)	0.086 (6.7)	0.12	0.005 (1.3)	0.115 (7.6)
Hexenes	0.01	0.006 (3.6)	0.004 (0.3)	0.017	0.013 (3.7)	0.004 (0.26)
Heptanes	0.028	0.018 (11.1)	0.01 (0.75)	0.046	0.051 (14.6)	−0.005 (0.0)
Heptenes	0.014	0.011 (6.4)	0.003 (0.27)	0.035	0.01 (2.8)	0.025 (1.6)
Octanes	0.065	0.013 (7.9)	0.052 (4.1)	0.029	0.015 (4.2)	0.014 (0.9)
Isomers	0.785	0.016 (9.5)	0.769 (60.1)	0.84	0.016 (4.7)	0.82 (54.1)
Benzene	0.008	0.002 (0.9)	0.006 (0.5)	0.018	0.003 (1.0)	0.015 (0.9)
Toluene	0.035	0.016 (9.9)	0.019 (1.5)	0.062	0.031 (9.1)	0.031 (2.0)
(*m* + *p*)-Xylene	0.042	0.017 (10.4)	0.025 (1.9)	0.045	0.017 (4.9)	0.028 (1.8)
Total	1.45	0.17	1.28	1.86	0.35	1.5
Distribution (wt%)						
Isomers (I)	54.2	9.5	60.1	45.1	4.7	54.1
Cracking (C)	39.9	69.3	36.0	48.2	80.3	41.2
Aromatics (A)	5.9	21.2	3.9	6.7	15	4.7
Molar ratios						
iC_4/nC_4	4.9	0.7	10.4	3.4	0.7	9.2
C_3/C_4	0.8	1.15	0.7	1.0	1.2	0.9
C_2/C_5	0.4	1.4	0.3	0.5	1.0	0.4
Alkenes/alkanes	0.2	0.7	0.2	0.3	0.6	0.2
Alkanes/benzenics	8.3	3.4	11.2	9.8	6	12.4

3.4.2. Catalytic role of sinusoidal channels

After successive deactivation of the HMCM22 sample by mX transformation for 10 h and poisoning by 2,4-DMQ added to the mch reactant, the conversion rate of pure mch was very low (Table 6). This indicates that the sinusoidal channels played a very limited role in mch transformation, only ∼2% of the total transformation into desorbed products. Furthermore, no deactivation was observed. Therefore, to estimate the product distribution at low X values with good accuracy, experimental points obtained at three different TOS values were considered for each contact time.

Comparing columns 2 and 5 of Table 6 with columns 3 and 6 of Table 5 (values in brackets) reveals significant differences in mch transformation within the sinusoidal channels and the supercages:

- I, C, and A distribution largely in favour of C products in the sinusoidal channels (70–80%) and I products in the supercages (value extrapolated at zero conversion of 55%).
- Completely different distribution of the C products and A products. The supercage C products constituted C_2–C_6 products (essentially C_3–C_5), whereas those formed in the sinusoidal channels constituted C_1–C_8 hydrocarbons (essentially C_3, C_4, and C_7) (Fig. 12). Moreover, in the sinusoidal channels, the branching was more limited, for example, iC_4/nC_4 of ∼0.7 instead of ∼8 in the supercages; the molar C_2/C_5 and C_3/C_4 ratios were close to 1 instead of 0.2–0.4; the olefin/paraffin molar ratio was higher, 0.6–0.7 instead of 0.03; and the paraffin to aromatic ratio was much smaller, 3–6 instead of >30 in the supercages. It should be noted that the C_5–C_7 olefinic products that did not appear in the distribution found on the fresh zeolite likely correspond to the products appearing in negative amounts in the supercage distribution (Table 5). Furthermore, the aromatic products A formed in the sinusoidal channels contain essentially toluene plus smaller amounts of benzene and xylenes, instead of essentially xylenes plus toluene in the supercages.

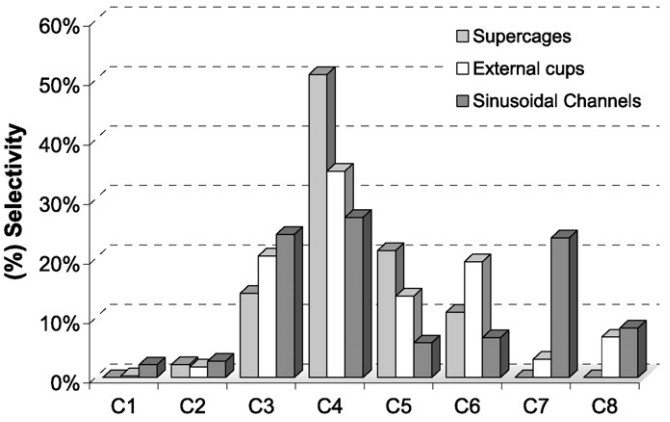

Fig. 12. C_1–C_8 cracking products distribution within the supercages, external cups and sinusoidal channels.

Consequently, the mode of mch transformation was completely different in the sinusoidal channels than in the supercages (Scheme 1). An important finding is that the product distribution for the sinusoidal channels was close to that found at 350 °C with a HMFI zeolite (P. Matias, unpublished results), typical for average pore size zeolites.

Scheme 3 presents the most likely reactions accounting for formation of the main products within the MCM22 sinusoidal channels:

The first steps of this transformation probably are protolytic dehydrogenation and cracking of methylcyclohexane. These mono-

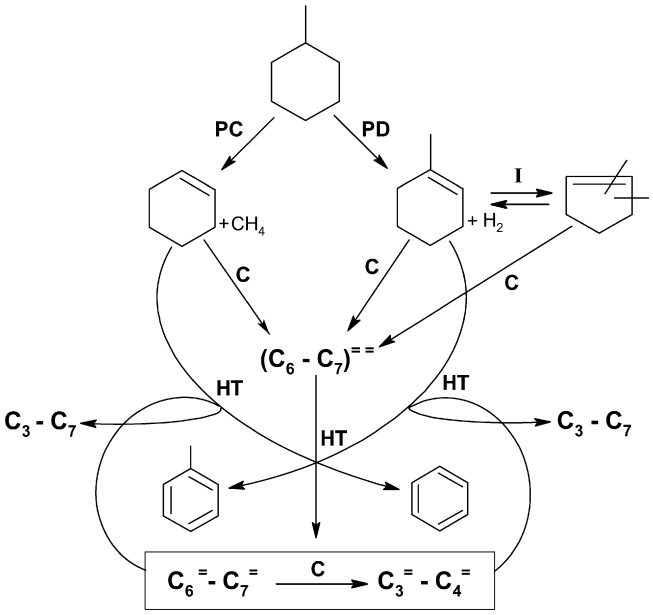

Scheme 3. Main steps of methylcyclohexane transformation in the sinusoidal channels: PC, PD: protolytic cracking and dehydrogenation; C: cracking; I: isomerisation; HT: hydrogen transfer.

molecular reactions are favoured because the formation of bimolecular transition states involved in the carbenium ion chain mechanism is sterically limited in the narrow sinusoidal channels. Protolytic mch dehydrogenation and cracking lead to methylcyclohexene ($+H_2$) and to cyclohexene ($+CH_4$),

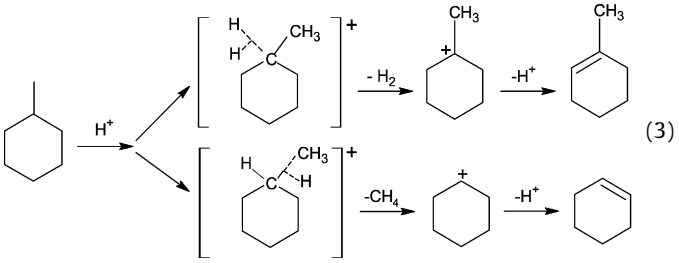

(3)

These olefins, which are highly reactive can undergo various reactions, particularly skeletal isomerisation into dimethyl, ethyl, and methyl cyclopentenes, with all of the cyclohexenic and cyclopentenic compounds leading to heptadiene or hexadiene products by cracking. Hydrogen transfer reactions from cyclohexenic molecules to these dienic products lead to benzene, toluene, and heptene, hexene, heptane, and hexane products. Heptene and hexene products also can be cracked into propene plus butene and into two propene molecules, respectively. All of these light olefins participate in hydrogen transfer reactions with the formation of propane and butanes. Finally, C_8 hydrocarbons could result from dimerisation-cracking of olefinic and diolefinic C_6 and C_7 hydrocarbons.

3.4.3. Catalytic role of external cups

The mch conversion rate (X) and product yields in external cups are given by the difference between the values found after mX ageing for 10 h and after poisoning by 2,4-DMQ (Table 6). The distributions of the products formed in the external cups at contact time values, τ, of 0.065 and 0.13 h are reported in brackets in columns 3 and 6 of Table 6. The product distribution did not differ greatly from that found for the supercages: similar I, C, and A distributions at zero conversion (55–60 wt% of I, 35–40% of C, and 4–5% of A); limited differences in the distribution in size of the C (Fig. 12) and A products (Tables 5 and 6); and significant branching in the C products (iC_4/nC_4 = 8–10). The most apparent differences involve the higher value of the olefin/paraffin, C_3/C_4, and C_2/C_5 molar ratios and the presence of small amounts of C_7 and C_8 products. These differences are in agreement with the lesser significance of the secondary reactions: cracking, dimerisation-cracking, and hydrogen transfer.

3.4.4. Effect of the pore system on the activity and selectivity of the acid sites

The rates of the main types of reactions—isomerisation (I), cracking (C), and aromatisation (A)—in each of the three pore systems (Table 7) were estimated from the rate values reported in Table 2 and from the product distribution in each system extrapolated at zero conversion. Furthermore, because apparently no deactivation of the sinusoidal channels and of the outer hemicages occurred, coking was found to occur only within the supercages.

From the rate values and the concentration of protonic acid sites in each location, the activities of the protonic sites (turnover frequency [TOF]) were determined. The acidity values were deduced from (i) C_{Bt}, the total concentration of protonic sites retaining pyridine adsorbed at 150 °C as pyridinium ions; (ii) C_{Bext}, the concentration of hemicage protonic sites; and (iii) the distribution of the bridging OH groups (and thus of the protonic sites) between supercages, sinusoidal channels, and hexagonal prisms. For sake of simplification, these latter sites, which may be accessible from both supercages and sinusoidal channels [37], were considered in equal amounts in each of these pore systems. The following acidity values were obtained: 478 $\mu mol\,g^{-1}$ in supercages, 151 $\mu mol\,g^{-1}$ in sinusoidal channels, and 25 $\mu mol\,g^{-1}$ in outer hemicages. Estimated TOF values based on the hypothesis that all of the sites assumed to be in hexagonal prisms actually were in either supercages or sinusoidal channels gave similar results.

Table 7 shows that the TOF value of the hemicage sites was 2.5 times higher than that of the supercage sites and much higher (~40 times) than that of the sinusoidal channels. The low activity of these latter sites is possibly related to significant steric constraints in the narrow channels or channel intersections. It also could be due to limitations in the diffusion of methylcyclohexane molecules, however, as suggested by experiments of methylcyclohexane adsorption; at 298 K, methylcyclohexane molecules probably cannot enter the sinusoidal channels [44]. The TOF values of the protonic sites of the outer hemicages and of the supercages were ~7 and 18 times lower, respectively, than those of the USHY sites [39], possibly related to the lower acid strength or confinement effect (hemicages) and to diffusion limitations (supercages).

4. Conclusion

The catalytic roles of the acidic sites of supercages, sinusoidal channels, and outer hemicages in methylcyclohexane transformation were investigated through an approach previously used to evaluate xylene transformation. This method is based on the selective deactivation by coking of supercages, which are typical trap cages (large cages with narrow apertures), and of the acid sites of the outer hemicages by poisoning with a bulky basic molecule (2,4-dimethylquinoline). The reaction products can be classified into four categories: dimethyl and ethyl cyclopentane isomers (I); C_2–C_8 aliphatic hydrocarbons, either olefinic or paraffinic (C); benzenic compounds (A), essentially benzene, toluene, and xylenes; and carbonaceous compounds (coke).

On the fresh catalyst, >85% of methylcyclohexane transformation occurred within the supercages, along with formation of similar amounts of isomers (I), C_3–C_5 branched paraffins (C), and trapped carbonaceous compounds (coke) through the classical carbenium ion chain mechanism. The formation of the C and coke

Table 7
Rate (mmol g^{-1} h^{-1}) of the main reactions: isomerisation (I), cracking (C), aromatisation (A) and coking in the three pore systems of the fresh MCM-22 zeolite and turnover frequency (TOF, h^{-1}) values in brackets

Location	Rate (TOF)				
	Total	I	C	A	Coking
Supercages	15.65 (33)	5.5 (11.5)	4 (8.4)	0.45 (1)	5.7 (12)
Sinusoidal channels	0.25–0.35 (2)	0.02–0.03 (0.2)	0.2–0.3 (1.6)	0.05 (0.35)	0 (0)
External cups	2–2.1 (82)	1.1 (44)	0.8 (32)	0.1 (4)	0 (0)
Total (MCM-22)	18.0 (28)	6.6 (10)	5.10 (8)	0.6 (1)	5.7 (9)

products required numerous steps, due to the long residence time of the molecules within these trap cages (large cages with small apertures) because of desorption limitations. The carbonaceous deposits caused rapid deactivation of the supercages.

In contrast, no deactivation—and thus no coke formation—occurred in methylcyclohexane transformation within the sinusoidal channels and the outer hemicages. This behaviour, reported previously for xylene transformation, can be explained by the inability to form and retain heavy products.

Less than 2% of methylcyclohexane transformation occurred within the sinusoidal channels with essentially formation of C_1–C_8 aliphatic hydrocarbons. The presence of methane indicates the participation of protolytic mechanisms in catalytic cracking. This participation, as well as the low reactivity of methylcyclohexane, could be related to severe steric constraints in this narrow pore system with inhibition of the bimolecular reactions and thus of the carbenium ion chain mechanism as well. Limitations in the diffusion of methylcyclohexane molecules also could be responsible for the low reactivity. With the fresh zeolite sample, most of the C_6–C_8 olefinic products formed in the sinusoidal channels were rapidly transformed in the supercages.

More than 10% of methylcyclohexane transformation was catalysed by the protonic sites of the outer hemicages. The distribution of the desorbed products was relatively close to that found with supercages but with fewer successive reactions, as expected due to the open shape of these micropores. On the hemicage sites, the TOF for the formation of the I and C products was ∼4 times greater than on the supercage sites but ∼7 times less than on USHY zeolite sites, due to their lower strength and/or a more limited confinement effect.

Significant similarities were seen between the behaviour of MCM22 in methylcyclohexane and xylene transformations [25]. In particular, the protonic sites of the outer cups were more active (i.e., 2–3 times greater TOF values) than those of the supercages. Furthermore, as was found with *o*-xylene [25], the protonic sites of the sinusoidal channels were practically inactive. These findings suggest that the influence of acid strength was less pronounced than that of micropore geometry. A particularity of methylcyclohexane transformation related to the large number and variety of possible reactions merits mention: Some of the products formed within a micropore system can undergo secondary transformations in another one.

Acknowledgments

P. Matias thanks the Fundação para a Ciência e Tecnologia (FCT) of Portugal for its financial support (Ref. SFRH/BD/19843/2004). The authors gratefully acknowledge P. Ayrault for the FTIR experiments and C. Canaff for the mass spectrometry analysis of coke, from the Laboratoire de Catalyse en Chimie Organique (LACCO).

References

[1] M.E. Leonowicz, S.L. Lawton, R.D. Partridge, P. Chen, M.K. Rubin, Science 264 (1994) 1910.
[2] S.L. Lawton, M.E. Leonowicz, R.D. Partridge, P. Chen, M.K. Rubin, Microporous Mesoporous Mater. 23 (1998) 109.
[3] J.S. Beck, A.B. Dandekar, T.F. Degnan, in: M. Guisnet, J.P. Gilson (Eds.), Zeolites for Cleaner Technologies, in: Catalytic Science Series, vol. 3, Imperial College Press, London, 2002, p. 223.
[4] A. Corma, C. Corell, F. Llopis, A. Martinez, J. Perez-Pariente, Appl. Catal. A 115 (1994) 121.
[5] W. Souverijns, W. Verrelst, G. Vanbutsele, J.A. Martens, P.A. Jacobs, J. Chem. Soc. Chem. Commun. (1994) 1671.
[6] A. Corma, J. Martinez-Triguero, J. Catal. 165 (1997) 102.
[7] P. Wu, T. Komatsu, T. Yashima, Microporous Mesoporous Mater. 22 (1998) 343.
[8] L. Liu, M. Cheng, D. Ma, G. Hu, X. Pan, X. Bao, Microporous Mesoporous Mater. 94 (2006) 304.
[9] X. Ren, J. Liang, J. Wang, J. Porous Mater. 13 (2006) 353.
[10] H.G. Karge, S. Ernst, M. Weihe, U. Weiß, J. Weitkamp, in: J. Weitkamp, H.G. Karge, H. Pfiefer, W. Hölderich (Eds.), Zeolites and Related Microporous Materials: State of the Art 1994, in: Stud. Surf. Sci. Catal., vol. 84, Elsevier, Amsterdam, 1994, p. 1805.
[11] Se-Ho Park, H-Ku Rhee, Appl. Catal. A 219 (2001) 99.
[12] J.M. Silva, M.F. Ribeiro, F. Ramôa Ribeiro, E. Benazzi, M. Guisnet, Appl. Catal. A 125 (1995) 15.
[13] S. Inagaki, K. Kamino, E. Kikuchi, M. Matsukata, Appl. Catal. A 318 (2007) 22.
[14] D. Nuntasri, P. Wu, T. Tatsumi, J. Catal. 213 (2003) 272.
[15] E. Dumitriu, D. Meloni, R. Monaci, V. Solinas, C. R. Chim. 8 (2005) 441.
[16] J.T.F. Degnan, C. Morris Smith, R. Chaya Venkat, Appl. Catal. A 221 (2001) 283.
[17] C. Perego, P. Ingallina, Catal. Today 73 (2002) 3.
[18] A. Corma, V. Fornés, L. Forni, F. Márquez, J. Martínez-Triguero, D. Moscotti, J. Catal. 179 (1998) 451.
[19] Se-Ho Park, H-Ku Rhee, Catal. Today 63 (2000) 267.
[20] A. Corma, V. Martínez-Soria, E. Schnoeveld, J. Catal. 192 (2000) 163.
[21] H. Du, D.H. Olson, J. Phys. Chem. B 106 (2002) 395.
[22] S. Laforge, D. Martin, M. Guisnet, Microporous Mesoporous Mater. 67 (2004) 235.
[23] J. Rigoreau, S. Laforge, N.S. Gnep, M. Guisnet, J. Catal. 236 (2005) 45.
[24] S. Laforge, D. Martin, J.L. Paillaud, M. Guisnet, J. Catal. 220 (2003) 92.
[25] S. Laforge, D. Martin, M. Guisnet, Appl. Catal. A 268 (2004) 33.
[26] H.S. Cerqueira, P.C. Mihindou-Koumba, P. Magnoux, M. Guisnet, Ind. Eng. Chem. Res. 40 (2001) 1032.
[27] A. Corma, C. Corell, J. Pérez-Pariente, Zeolites 15 (1995) 2.
[28] G. Leofanti, M. Padovan, G. Tozzola, B. Venturelli, Catal. Today 41 (1998) 207.
[29] W.D. Harkins, G. Jura, J. Chem. Phys. 11 (1943) 431.
[30] M.M. Dubinin, L.V. Radushkevich, Proc. Acad. Sci. USSR 55 (1947) 331.
[31] F. Rouquérol, J. Rouquérol, K.S.W. Sing, Adsorption by Powders and Porous Solids, Academic Press, London, 1999.
[32] M. Guisnet, P. Ayrault, J. Datka, Pol. J. Chem. 71 (1997) 1455.
[33] P. Ayrault, J. Datka, S. Laforge, D. Martin, M. Guisnet, J. Phys. Chem. B 108 (2004) 13755.
[34] M. Guisnet, P. Magnoux, Appl. Catal. A 54 (1989) 1.
[35] B. Onida, L. Borello, F. Testa, F. Crea, E. Garrone, Microporous Mesoporous Mater. 30 (1999) 119.
[36] D. Meloni, S. Laforge, D. Martin, M. Guisnet, E. Rombi, V. Solinas, Appl. Catal. A 215 (2001) 55.
[37] D. Meloni, D. Martin, M. Guisnet, Appl. Catal. A 215 (2001) 67.
[38] H. Ja Jung, S.S. Park, C-Ho Shin, Y-Ki Park, S.B. Hong, J. Catal. 245 (2007) 65.
[39] G. Caeiro, Ph.D. thesis, Universidade Técnica de Lisboa/Université de Poitiers, 2006, p. 58.
[40] M. Guisnet, P. Magnoux, Appl. Catal. A 212 (2001) 83.
[41] E. Besset, D. Meloni, D. Martin, M. Guisnet, L. Schreyeck, in: B. Delmon, et al. (Eds.), Catalyst Deactivation, in: Stud. Surf. Sci. Catal., vol. 126, Elsevier, Amsterdam, 1999, p. 171.
[42] H.S. Cerqueira, P. Ayrault, J. Datka, M. Guisnet, Microporous Mesoporous Mater. 38 (2000) 197.
[43] G. Caeiro, Patrick Magnoux, J.M. Lopes, F. Ramôa Ribeiro, Appl. Catal. A 292 (2005) 189.
[44] P.A. Russo, M.M.L. Ribeiro Carrott, P.J.M. Carrott, P. Matias, J.M. Lopes, M. Guisnet, F. Ramôa Ribeiro, Microporous Mesoporous Mater. (2008), submitted for publication.